Supporting Online Material

I. Circuit Calibration and Data Analysis

Figure S1

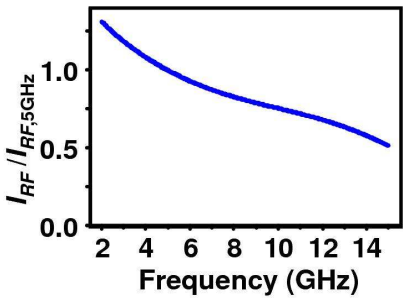

The RF attenuation in our cables, the bias tee, and the ribbon bonds connecting to the sample is frequency dependent. In order to know the value of I_{RF} at the sample, this attenuation must be calibrated. We calibrate the attenuation of the cables and bias tee by measuring their transmission with a network analyzer. To estimate the losses due to the ribbon bonds, we measure the reflection from ribbon-bonded open, short, and 50-Ω test samples. We observe negligible reflection from the bonded 50 Ω sample, implying that the ribbon bonds produce little impedance discontinuity for frequencies < 15 GHz. We can therefore estimate the frequency-dependent transmission through the ribbon bonds as the square root of the measured reflection coefficient from either the bonded open test sample or the bonded short (a square root because the reflected power travels twice through the ribbon bonds). Finally, we measure the reflection coefficient directly for each of our ribbon-bonded samples before collecting FMR data, and from this determine its impedance and the resulting value of I_{RF}. For the 30×90 nm^2 sample on which we focus in the paper, the frequency dependence of I_{RF} at the sample, referenced to the value at 5 GHz, is shown in Fig. S1.

The mixing signal contains a background due to deviations from linearity in the *I-V* curve of the sample, which we subtract from the data presented in the figures.

The thicknesses of the layers composing our samples are, from bottom to top, 120 nm Cu / 20 nm Py / 12 nm Cu / 5.5 nm $Ni_{81}Fe_{19}$ / 2 nm Cu / 30 nm Au, with a Au top contact. The difference in resistance between parallel and antiparallel magnetic layers for our 30×90 nm^2 sample at 10 K is ΔR_{max} = 0.84 Ω.

II. Peak Shape Analysis for Spin-Transfer-Driven FMR

In order to analyze our FMR peak shapes, we make the simplifying assumption that the lowest-frequency modes A_0 and B_0 can be approximated by a macrospin model, using the Landau-Lifshitz-Gilbert (LLG) equation of motion with the Slonczewski form of the spin-transfer torque [1]:

$$\frac{d\hat{m}}{dt} = \gamma\mu_0(\vec{H} + \vec{H}_{anis}) \times \hat{m} + \alpha\hat{m} \times \frac{d\hat{m}}{dt} + c\frac{\eta I(t)}{e}\hat{m} \times (\hat{m} \times \hat{M}). \qquad \text{(S1)}$$

Here $\hat{m}$ describes the moment direction of the precessing magnetic layer, γ is the gyromagnetic ratio, $\vec{H}_{anis}$ accounts for shape anisotropy, α is the Gilbert damping, η is a dimensionless efficiency factor, $\hat{M}$ is the moment direction of the static layer, and c = +1 for precession of the PyCu layer and –1 for precession of the Py layer. We consider the case of small-angle precession of the PyCu moment about $\hat{z}$. When $\hat{m}$ is initially at rest and I_{RF} is applied to excite FMR, Eq. (3) predicts that the resulting resonance is Lorentzian

$$V_{mix}(f) = \frac{\eta c I_{RF}^2 \Delta R_{max} \sin^2(\theta_{stat})}{16\pi\Delta_0 e}\left(\frac{1}{1+[(f-f_0)/\Delta_0]^2}\right), \qquad \text{(S2)}$$

where θ_{stat} is the angle between $\hat{M}$ and the precession axis, f_0 is the unforced precession frequency, and the width Δ_0 is

$$\frac{\Delta_0}{f_0} = \alpha \frac{H/M_s - N_z + N_x/2 + N_y/2}{\sqrt{(H/M_s - N_z + N_x)(H/M_s - N_z + N_y)}}. \quad \text{(S3)}$$

We estimate that the effective demagnetization factors for our PyCu layer are N_z = 0.79, N_x = 0.03, and N_y = 0.18, based on a magnetization of 0.39 T [2] and coercive field measurements. However, the result of Eq. (5) is quite insensitive to these values, so that for $\mu_0 H$ > 0.5 T we have simply $\Delta_0/f_0 = \alpha$ for the PyCu layer to within 1% error. Simulations show that this prediction is also not altered at the 1% level by the 5º offset between $\vec{H}$ and the $\hat{z}$ direction in our measurements.

For the Py layer mode, there is an additional correction required to relate Δ_0 / f_0 to α, due to the larger deviation of the precession axis from $\hat{z}$.

III. Simulation Parameters

In our numerical simulations, we integrate the LLG equation for macrospin precession (Eq. (S1)), using the following parameters: α = 0.04, g = 2.2, a PyCu magnetization $\mu_0 M_s$ = 390 mT [2], in- and out-of-plane anisotropies 58 mT and 300 mT, and an efficiency parameter $\eta = (0.2) g\mu_B/(2M_s V)$, where μ_B is the Bohr magneton and V is the volume of a 5.5-nm-thick disk of elliptical cross section 90 × 30 nm^2. Thermal effects are modeled with a 10 K Langevin fluctuating field [3]. For Fig. 3(d), I_C = 0.6 mA, f_0 = 8.1 GHz, and I_{RF} = 0.1-1, 1.2, 1.5, 2, 3, and 4 mA. The qualitative results of the simulation are not affected by reasonable variations in device parameters.

IV. Regarding another proposed mechanism for DC voltages produced by magnetic precession:

Berger has proposed that a precessing magnet in a multilayer device may generate a DC voltage directly [4]. This mechanism could produce another source of signal in our experiments on resonance, in addition to the mixing mechanism we discussed in the main text. However, the maximum magnitude of V_{DC} predicted to be generated by the Berger mechanism is $hf/e = 40\ \mu$eV for f = 10 GHz, and our FMR signals can grow much larger than this. Also, we find that at small values of I_{RF} our signals scale as $V_{DC} \propto I_{RF}^2$ as expected for the mixing mechanism (because $\left|\Delta R_f\right| \propto I_{RF}$), while the Berger signal would scale $\propto I_{RF}$. On this basis, we argue the mixing mechanism is dominant in producing our signal, and we have considered only this mechanism in our analysis.

References:

1 J. C. Slonczewski, *J. Magn. Magn. Mater.* **159**, L1 (1996).

2 R. Watts, D. K. Wilkinson, I. R. Barkshire, M. Prutton, A. Chambers, *Phys. Rev. B* **52**, 451 (1995).

3 W. F. Brown, *Phys. Rev.* **130**, 5 (1963).

4 L. Berger, *Phys. Rev. B* **59**, 11465 (1999).